The use of *in situ* cosmogenic ^{21}Ne in studies on long-term landscape development

Abstract

Cosmogenic Ne isotopes are stable and are routinely used for constraining the timing of events and the rate of surface change beyond the limit that can be studied with the radionuclides ^{10}Be, ^{26}Al and ^{36}Cl. In addition to quartz it can be used in a range of other minerals. Analysis typically requires significantly less material than for cosmogenic ^{10}Be and ^{26}Al opening up the technique for small samples, for example, individual pebbles in river sediments. Analysis is easier and faster than for the radionuclides, not least because Ne measurements do not require significant chemical procedures. However, the presence of other sources of Ne in minerals tends to restrict the use of cosmogenic ^{21}Ne to old landscapes and long exposure durations. In this review we briefly outline the background to cosmogenic Ne production in rocks and minerals at the Earth's surface, then documents the key uses of the technique by highlighting some earlier studies, and finishes with a short perspective on the future of the technique.

Keywords: cosmogenic nuclides, ^{21}Ne, long timescale, landscape evolution.

1. Introduction

The last two decades has seen the development of routine techniques for determining the concentration of cosmogenic nuclides in terrestrial rocks and minerals. The widespread application of, in particular, the cosmogenic radionuclides has led to a step change in knowledge of the timing and rates of Earth surface processes (Gosse and Phillips 2001). The headline applications of the technique has included the precise determination of deglaciation timescales (e.g., Ivy-Ochs et al. 2006), the slip history of faults (e.g., Benedetti et al. 2002), the erosion rate of river catchments (e.g., Portenga and Bierman 2011) and the time of sediment burial in order to determine rates of landscape evolution (e.g., Granger and Riebe 2007).

The vast majority of terrestrial cosmogenic nuclide studies have exploited the radioactive nuclide

^{10}Be in quartz. The stable cosmogenic nuclides ^{3}He and ^{21}Ne have higher production rates than the radionuclides, and can be measured on conventional gas source mass spectrometers that are significantly less expensive and require less manpower to operate than accelerator mass spectrometers (AMS) required for radionuclides. Despite this they have been exploited far less routinely. This is in large part due to the presence of other sources of ^{3}He and ^{21}Ne in minerals that must be quantified precisely prior to successful application of the technique. Diffusive loss of cosmogenic ^{3}He from quartz limits the technique to mafic minerals such as olivine, pyroxene and FeO (e.g., Foeken et al. 2009; Margerison et al. 2005). Despite this restriction it has had a broad range of applications; from constraining the evolution of Cenozoic ice history of Antarctica (Kong et al. 2010; Margerison et al. 2005) and the topographic evolution of mountain belts (Evenstar et al. 2015), to determining the timing of the collapse of volcanic edifices in the Holocene (Foeken et al. 2009). Cosmogenic ^{21}Ne is retained in quartz. As well as providing a useful compliment to cosmogenic radionuclides, ^{21}Ne has proved to be a powerful tracer of long-term landscape change of, in particular, slowly eroding landscapes.

In this paper we first review all aspects of the production of cosmogenic ^{21}Ne in minerals at the Earth's surface, then discuss the techniques that are commonly used for Ne isotope measurement. This is followed by a short explanation of the complications generated by the production of Ne by nuclear reactions in minerals, and trapped air-derived Ne. It finishes with an overview on the recent advances in the application of cosmogenic ^{21}Ne to long-term landscape development. This is separated into two sections; studies that concentrate on exposure age determinations and those that aim to quantify erosion rates.

2. Background

2.1 Production of terrestrial in-situ cosmogenic isotopes

The terrestrial in-situ produced cosmogenic nuclides are generated by interactions of secondary cosmic-ray particles with the target nuclei in the minerals near the Earth's surface. There are three main nuclide production pathways: (i) spallation reaction by fast- and high-energy secondary cosmic ray particles, where neutrons are the dominant particle. The intensity of neutrons is attenuated

exponentially in the rock due to nuclear interactions and ionization losses (Lal and Peters 1967). The attenuation of energy and flux of the cosmic-ray particles provides the possibility for the studies of surficial processes with *in situ*-produced cosmogenic nuclides, whose production rates beneath rock surface are dependent on the intensity of neutrons and can be modeled by an exponential function with depth in the surface material (Lal 1991). (ii) negative muon capture and (iii) fast muon-induced reactions. The negative muon-induced production is only significant at the depth of 2.5-3 m in most rocks, where the high-energy neutron flux is less than 1% of the surface. Fast muons have sufficiently high energy to cause neutron reactions, but due to their very low abundance they are only become important at great depth when no other secondary cosmic-ray particles survive. Muon-induced reactions contribute only a few percent to the total cosmogenic nuclide production in the surface rocks of the Earth (e.g., Borchers et al. 2016; Braucher et al. 2011; Marrero et al. 2016).

Due to atmospheric and geomagnetic shielding the cosmic ray particle flux, and therefore cosmogenic nuclide production rates at the Earth's surface, vary with altitude and geomagnetic latitude. Consequently the rate of nuclide production has to be scaled with the variation of latitude and elevation. Scaling is mainly based on measurements of the present day cosmic ray flux. The first model was based on photographic records of spallation events in photo-emulsions (Lal 1991). This model has been modified subsequently to take account of the effect of pressure (Balco et al. 2008; Stone and Vasconcelos 2000). The majority of scaling models are based on the global neutron monitor network that is maintained by the cosmic-ray physics community (Desilets and Zreda 2003; Desilets et al. 2006; Dunai 2001; Lifton et al. 2005). These models scale production with altitude in regions of high magnetic strength. Most recently, Lifton et al. (2014) have used numerical simulations of cosmic-ray modulation by the geomagnetic field and the atmosphere calibrated using atmospheric differential flux measurements for neutrons and protons. Collectively these models produced small differences in cosmogenic nuclide production rates. Production rates are typically normalized to sea level high latitude (SLHL).

The measurement of absolute production rates of the commonly-used cosmogenic nuclides are generally done using natural calibration sites, where the accumulated cosmogenic nuclide concentration is measured in a rock surface of known age (e.g., Balco and Shuster 2009b). These

calibration sites must be old enough to have accumulated measureable nuclide concentrations, but must be young enough to have avoided significant degradation by weathering and erosion. Phillips et al. (2016) reviews the prevailing radionuclide calibration studies and introduces cosmogenic ^{10}Be, ^{26}Al and ^{36}Cl data for four new calibration sites that were selected by the CRONUS-Earth project. Goehring et al. (2010) reviewed the prevailing calibration sites for ^{3}He production rate, though work is ongoing (Foeken et al. 2012).

2.2 Cosmogenic neon

Neon has three stable isotopes, ^{20}Ne, ^{21}Ne and ^{22}Ne, of which ^{20}Ne is the most abundant in atmosphere (90.50%). All three neon isotopes are produced at similar rates by cosmic ray secondary neutron spallation reactions in rocks. Due to the lower natural abundance in air, ^{21}Ne and ^{22}Ne concentrations are most sensitive to the cosmogenic production in minerals. Cosmogenic ^{21}Ne is generally adopted as the parameter to reflect the surface exposure history as the production rate is high in comparison to the amount present in minerals.

Cosmogenic Ne isotopes are produced largely from the target elements Na, Mg, Al and Si, as these have the largest reaction cross-sections and are closest in mass to Ne. Cosmogenic Ne is quantitatively retained by most silicates (Shuster and Farley 2005). The ubiquity of quartz at the Earth surface means it is the dominant target mineral, but olivine and pyroxene are used in studies of igneous rocks.

Atmosphere-derived Ne is ubiquitous in minerals. At its simplest, the Ne isotope composition of surface exposed minerals reflects the two-component mixture of atmospheric and cosmogenic neon. This mixing line is defined by the "spallation line" in the Ne three-isotope diagram (Fig. 1). The slope of the spallation line depends on the mineral composition, and the cosmogenic ^{21}Ne/^{22}Ne values determined experimentally for quartz are 1.120 ± 0.020 (Niedermann et al. 1993) and 1.143 ± 0.038 (Schäfer et al. 1999). The corresponding value for pyroxene is similar, 1.055 ± 0.017 (Bruno et al. 1997).

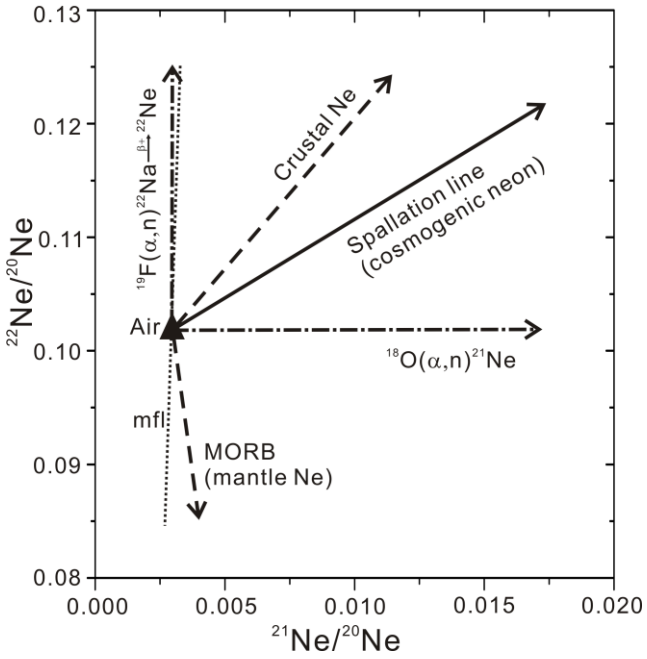

Fig. 1 Neon three-isotope diagram ($^{22}Ne/^{20}Ne$ *vs.* $^{21}Ne/^{20}Ne$) showing the compositions and trends of various Ne components (Niedermann 2002) mfl: mass fractionation line

Determining the production rate of cosmogenic ^{21}Ne isotope is more difficult than the radionuclides and ^{3}He, due to the relatively low production rate compared to atmosphere concentration in minerals. The first determination of cosmogenic ^{21}Ne production rate in quartz was reported by Niedermann et al. (1994). Based on the production rate ratios of $^{21}Ne/^{26}Al$ (0.65 ± 0.11), which was considered to be equal to the nuclide concentration ratio in the short exposed quartz samples (assuming an age of 11 ka based on radiocarbon dates from the work of Nishiizumi et al. (1989)) collected from the glacially polished granite surface at Sierra Nevada, California, the cosmogenic ^{21}Ne production rate was determined to be 21 atoms g^{-1} a^{-1}. These authors managed to distinguish the various neon components containing in the Sierra Nevada rock samples by isotopic signatures and release systematics. They measured all three neon isotopes in stepwise gas extraction to evaluate the cosmogenic neon, trapped components including the atmospheric, as well as inherited components. The nucleogenic neon impacted the precision of the measurement of the extremely low concentration of cosmogenic neon in this short exposed quartz samples, nevertheless, authors have shown a $^{21}Ne/^{26}Al$ ratio with an uncertainty of 17%. Niedermann (2000) revised the rate to 19.0 ± 3.7 atoms g^{-1} a^{-1} after adopting a revised exposure age of 13 ka (Clark et al. 1995), and used the geomagnetic latitude of the sampling

site for scaling the production rate to SLHL.

According to the latest report about the cosmogenic nuclide production rate calibration (Phillips et al. 2016), the SLHL production rate of ^{10}Be, which is converted from the primary calibration site production rate using Lal-Stone scaling method, is determined to be 4.01 atoms g^{-1} a^{-1}. Based on this updated ^{10}Be production rate, cosmogenic ^{21}Ne production rate (SLHL) is revised to be 15.69 atoms g^{-1} a^{-1}.

Balco and Shuster (2009b) reported an independent determination of ^{21}Ne production rate in quartz. Instead of relying on a single calibration site with short exposure history, they selected sites in the Antarctic Dry Valleys where the surface ^{21}Ne concentration has reached steady state between nuclide production and loss by surface erosion. Relatively high cosmogenic nuclide concentrations allow the high accuracy of nuclide concentration ratio determination. Combining the steady-state surface concentrations ratio of ^{21}Ne/^{10}Be with the established ^{10}Be production rate of 4.61 atoms g^{-1} a^{-1}, they determined the total ^{21}Ne production rate to be 18.3 ± 0.4 atoms g^{-1} a^{-1} (SLHL) in quartz. Using the new ^{10}Be production rate (Phillips et al. 2016), the cosmogenic ^{21}Ne production rate (SLHL) is 15.9 atoms g^{-1} a^{-1} in quartz.

In the same year, Goethals et al. (2009a) used quartz collected from the surface of Bishop Tuff in eastern California with ^{40}Ar/^{39}Ar age of 760 ± 2 ka (Van den Bogaard and Schirnick 1995) to determine cosmogenic ^{21}Ne production rate. The precise exposure age of the tuff and its relatively high cosmogenic nuclide concentrations is crucial for the accuracy of nuclide production rate determination. The authors first measured concentrations of cosmogenic ^{10}Be and ^{21}Ne; then, based on the conservative estimate of the surface erosion rate using the tuff ^{40}Ar/^{39}Ar age and their previously published ^{21}Ne concentrations, they determined the ^{10}Be/^{21}Ne production rate ratio of assuming steady-state erosion. When combined with the production rate of ^{10}Be of 4.61 atoms g^{-1} a^{-1}, the production rate ratio converted to a quartz ^{21}Ne SLHL production rate of 19.9 atoms g^{-1} a^{-1}. Again, using the new ^{10}Be production rate (Phillips et al. 2016), ^{21}Ne production rate (SLHL) will be 17.3 atoms g^{-1} a^{-1}.

2.3 Calculation of the exposure ages and surface erosion rates

For stable cosmogenic nuclides, age determinations assume that the concentration of cosmogenic ^{21}Ne, $N(z,t)$, accumulates in the surface materials with the exposure age, t. At any subsurface depth z, the temporal evolution of $N(z,t)$ in the rock can be expressed as (Lal 1991):

$$\frac{\mathrm{d}N(z,t)}{\mathrm{d}t} = P(z,t) \qquad (1)$$

where $P(z,t)$ is the production rate of the cosmogenic nuclide at the depth below the rock surface, and the temporal variation of production rate due to solar activity or geomagnetic field changes is assumed to be negligible, i.e., $P(z,t) = P(z)$. By assuming the rates of nuclide production induced by both spallation reaction and muon reactions decrease exponentially with depth,

$$P(z) = P_{\mathrm{n}}(z) + P_{\mu}(z) = P_{\mathrm{n}}(0)\cdot \mathrm{e}^{-\rho z/\Lambda_{\mathrm{n}}} + P_{\mu}(0)\cdot \mathrm{e}^{-\rho z/\Lambda_{\mu}} \qquad (2)$$

where $P_{\mathrm{n}}(0)$ and $P_{\mu}(0)$ are the rates of nuclide production induced by spallation reaction and muon reaction, respectively, at the rock surface; ρ is the rock density; and Λ_{n} and Λ_{μ} are the attenuation length (g cm^{-2}) of the particles causing the spallation reaction and muon reaction, respectively. The value of Λ_{n} is determined by experiment and calculation, with the widely used value ranging from 157 to 167 g cm^{-2} (Masarik and Reedy 1995). The value of Λ_{μ} can be approximated as around 1300 g cm^{-2} (Barbouti and Rastin 1983; Brown et al. 1995), or using more accurate mathematical representations, including the interactions with both stopped and fast muons, reported by Granger and Smith (2000).

For eroding landforms, z is time dependent, and $z(t)$ can be defined using erosion rate on the surface, $\varepsilon(t)$, according to the following equation (Lal 1991; Niedermann 2002):

$$z(t) = \int_0^t \varepsilon(t)\cdot dt + const. \qquad (3)$$

Defining the initial shielding depth z_0 at time of t= 0, and considering a case of constant erosion rate, i.e. $\varepsilon(t) = \varepsilon$, then the depth at the time of t is $z(t) = z_0 - \varepsilon\cdot t$.

Then for the differential equation (1), we can obtain the solution for stable nuclide concentration at rock surface, $N(t)$ (Niedermann 2002):

$$N(t) = N(0) + \frac{\mathrm{P_n}(0)}{\rho\varepsilon/\Lambda_{\mathrm{n}}}\cdot(1-\mathrm{e}^{-\rho\varepsilon\cdot t/\Lambda_{\mathrm{n}}}) + \frac{\mathrm{P}_{\mu}(0)}{\rho\varepsilon/\Lambda_{\mu}}\cdot(1-\mathrm{e}^{-\rho\varepsilon\cdot t/\Lambda_{\mu}}) \qquad (4)$$

where $N(0)$ is the initial nuclide concentration in the rock at the moment t= 0 that inherited from all

previous exposure events.

Equation (4) illustrates the relationship of cosmogenic ^{21}Ne concentration with both exposure duration and erosion rate, which gives only the minimum exposure age and the maximum erosion rate from a measured cosmogenic nuclide concentration in a sample. The measurement of two cosmogenic nuclides with different half-lives in the same sample can be used to constrain exposure age and erosion rate. ^{21}Ne is commonly coupled with ^{10}Be as both can be measured in the same quart sample to investigate the history of old surfaces. The temporal evolution of the nuclide concentration ratio ^{21}Ne/^{10}Be for various erosion rates is plotted in Fig. 2, in which the area between the two curves, steady-state erosion island (Lal 1991), comprises all the possible combinations of steady-state erosion and simple exposure histories (Lal 1991; Niedermann 2002). However, complex exposure, e.g., periods of burial, will also change the ratio of the two nuclides due to ^{10}Be decay. This is shown in Fig. 2. In a situation that a surface experienced exposure, buried for a period, and re-exposed, the concentrations of the radionuclides ^{10}Be and ^{26}Al will return to equilibrium with the steady erosion if the re-exposure time is long enough, so the ^{10}Be/^{26}Al pair will lose the evidence of a complex exposure history. When adding ^{21}Ne measurement to ^{10}Be or ^{26}Al, ^{21}Ne concentration which is totally preserved and requires much longer time to reach steady state with the new erosion will retain the information about previous period of exposure and burial, as an evidence for recognizing complex exposure histories.

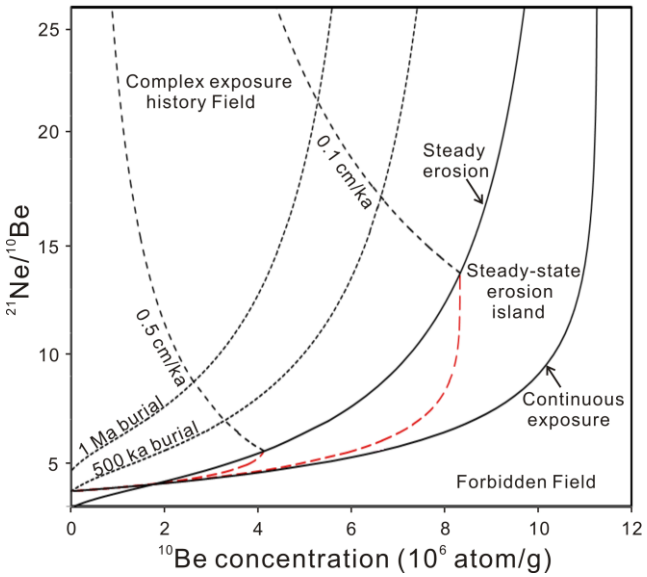

Fig. 2 Plot of the concentration ratio ^{21}Ne/^{10}Be versus the ^{10}Be concentration, generated using

CosmoCalc version 1.7 (Vermeesch 2007) using the production rate of 5.16 atom/g/a for ^{10}Be and 19.3 atom/g/a for ^{21}Ne. The lower solid line represents the temporal evolution of these two values in the continuous exposed surface without the effect of erosion, the upper solid line in steady-state erosion condition. Dash lines indicate the temporal evolution under erosion rates of 0.5 and 0.1 cm/ka; dotted lines under different burial periods of 1 and 0.5 Ma. The area between the "continuous exposure" curve and the "steady erosion" curve is "steady-state erosion island", which comprise all possible combinations of exposure ages and erosion rates for simple exposure histories

3. Measurement of cosmogenic ^{21}Ne

Cosmogenic Ne analysis is generally performed on between 5 mg and 1 g of pure mineral. Typically this is quartz, but olivine and pyroxene have been analysed fairly routinely. This compares to 5-30 g of quartz that are usually required for ^{10}Be and ^{26}Al determinations by AMS. Sample preparation is largely restricted to the physical extraction of a discrete mineral phase from rock. Separation relies on density methods (e.g. shaker table and heavy liquids) and magnetic techniques. The target mineral-rich fraction is usually inspected under a binocular microscope and contaminating grains are removed by hand. Chemical processing of mineral samples is typically restricted variations of the Kohl and Nishiizumi (1992) leaching procedure in order to remove the outer few 10's μm mineral which may have nucleogenic Ne generated by implanted particles and neutrons. Samples are typically ultrasonically cleaned in deionised water to remove traces of HF from mineral surfaces, then acetone to remove contaminating trace hydrocarbons.

Typical analysis amounts range from 10 to 250 mg of each sample, depending on the Ne concentration. Samples are typically wrapped in metal foil – Al, Pt or Nb – in order to handle in vacuum systems. Gas extraction is typically undertaken either in double-vacuum resistance furnaces (e.g., Codilean et al. 2008) or using near-visible wavelength lasers to heat mineral samples directly (Balco and Shuster 2009b). Samples are usually pumped to ultra-high vacuum levels for many hours, sometimes heating to 50-70°C, prior to analysis to remove absorbed atmospheric Ne.

Cosmogenic Ne is extracted by heating each sample in one step (typically 1300°C) or in several temperature steps in order to identify different Ne components. Active gases are removed by

exposure to hot metal surfaces, usually ZrAl getter pumps or Ti sublimation pumps. The heavy noble gases and residual active gases are absorbed on liquid nitrogen-cooled traps of either activated charcoal or sintered metal. Getter pumps operated at room temperature are used to absorb hydrogen. Helium is removed by absorbing the residual gases onto cryostatic cold head.

Neon isotope analysis is done in static mode using high-resolution magnetic sector mass spectrometers. These typically employ Nier-type electron impact ion sources tuned to optimise sensitivity for Ne ionisation. Ion beam intensities are measured using electron multiplier, usually in peak jumping mode. The mass spectrometers usually contain room temperature getter pumps and liquid nitrogen-cooled trap in order to minimize the contribution of interfering species during analysis.

On all but the latest high-resolution noble gas mass spectrometers isobaric interferences at mass 20, 21 and 22 require correction. This entails measurement of the abundances of masses 2, 16, 18, 19, 20, 21, 22, 40 and 44 were. Instrumental sensitivity and mass fractionation in the instrument is calculated from repeated analysis of aliquots of Ne in air. In many laboratories the CREU quartz standard (Ma et al. 2015; Vermeesch et al. 2015) is used as an internal check.

The abundance of cosmogenic ^{21}Ne ($^{21}Ne_c$) in samples is calculated assuming that all the measured ^{20}Ne ($^{20}Ne_m$) is atmospheric in origin from:

$$^{21}Ne_c = {}^{21}Ne_m \times \frac{\left[\left(^{21}Ne/{}^{20}Ne\right)_m - \left(^{21}Ne/{}^{20}Ne\right)_{air}\right]}{\left(^{21}Ne/{}^{20}Ne\right)_m} \qquad (5)$$

Unresolved contributions to ^{20}Ne occur as a result of $H_2{}^{18}O^+$, $^{40}Ar^{2+}$ and HF^+. Interference at *m/e* = 20 from $H_2{}^{18}O^+$ are calculated from the measurement of $H_2{}^{16}O^+$ at mass 18. The $^{19}F^+$ signal was constant in mass spectrometer background, blank, calibration and sample measurements indicating that the fluorine is dominantly in the mass spectrometer. The absence of an effect of $H^{19}F^+$ on blank measurements implies that it is unimportant for measurement of samples ^{20}Ne. The dominant interference at *m/e* = 20 came from $^{40}Ar^{2+}$. The charge state ratio $^{40}Ar^+/^{40}Ar^{2+}$ is governed by the partial pressure of H in the mass spectrometer ionization region. A first-order relationship between $^{40}Ar^+/^{40}Ar^{2+}$ and H^+ beam size is recorded in many laboratories. The aim is to ensure that partial pressure of H remains constant throughout the analysis periods. Correction for $^{12}C^{16}O_2{}^{2+}$ at *m/e* = 22

is calculated from measured mass 44 ($^{12}C^{16}O_2^+$) using CO_2^{2+}/CO_2^+ determined by repeated measurements interspersed with sample measurements. Correction for $^{63}Cu^{3+}$ at ^{21}Ne can be done by measuring $^{65}Cu^{3+}$.

Although all three isotopes of neon need to be measured when calculating the cosmogenic ^{21}Ne concentration, the uncertainty of measured cosmogenic ^{21}Ne concentration mainly derives from the error of ^{21}Ne isotope measurement, usually around 5%. In some cases of high ^{21}Ne content, the error can go down to ~3%, which is nearly the lower limiting for cosmogenic ^{21}Ne measurement uncertainty. In consequence, the measurement uncertainty is commonly larger for ^{21}Ne than for the radionuclide ^{10}Be or ^{26}Al. However, ^{21}Ne is a stable isotope, so it eliminates the uncertainty from the determination of the decay constant of the radionuclide, which is known as ~1% for ^{10}Be and ~3% for ^{26}Al (Balco and Shuster 2009a).

As to the precision of the final exposure age or erosion rate, it does not only depend on the precision of the parameters involved in data calculation, such as the measured isotope content, the decay constant of the isotope, the nuclide production rate and the scaling factor of production rate, but also depends on how well the model we adopt works in this situation, for example, the age uncertainty depends more on whether the assumption of the simple/complex exposure history is appropriate for what the sample has undergone. As a result, the total uncertainty is high in some geological situations if all error sources are considered, no matter for ^{21}Ne or for radionuclides. However, cosmogenic ^{21}Ne is produced and retained in a range of minerals and thus has the potential for constraining the timing of the exposure of surfaces that cannot be studied with ^{10}Be and ^{26}Al. Furthermore, the unique possibility of stable ^{21}Ne isotope for quantitative geomorphologic studies in the low-erosion region also endows it with huge potential to become a powerful tool which cannot be replaced by radionuclides or other techniques.

4. Neon isotope components in minerals

There are several sources of isotopically-distinct Ne in minerals that must be quantified before the concentration of cosmogenic Ne can be determined.

Air: Neon is present with a volume concentration of 18.2 ppm in air. It has three stable isotopes -

283 ^{20}Ne, ^{21}Ne and ^{22}Ne - and the atmospheric isotope ratio of ^{21}Ne/^{20}Ne and ^{22}Ne/^{20}Ne are 0.002959 ±
284 0.000022 and 0.1020 ± 0.0008, respectively (Eberhardt et al. 1965). Honda et al. (2015) recently re-
285 determined the atmosphere Ne isotope composition, in particular revising the ^{21}Ne/^{20}Ne to be
286 0.002905 ± 0.000003.

287 Atmospheric neon is ubiquitous in mineral samples, even those that have crystallised deep in Earth
288 with no contact with air. It is likely that much of the air-derived Ne in minerals is absorbed onto
289 mineral surfaces. However, extremely high concentrations are measured in quartz, often probably
290 present in fluid inclusions (Graf et al. 1991; Niedermann et al. 1993). The mixture of atmospheric
291 and cosmogenic neon in samples always lies on the "spallation line" in Fig. 1.

292 *Nucleogenic Ne*: Neon isotopes are produced by an array of nuclear reactions in minerals. The
293 dominant source of nucleogenic Ne is produced by (α, n) reactions with ^{18}O (^{21}Ne) and ^{19}F (^{22}Ne), and
294 (n,α) reactions with ^{24}Mg (^{21}Ne) and ^{25}Mg (^{22}Ne) (Graf et al. 1991; Niedermann et al. 1993). The α-
295 particles are generated by radioactive decay of U and Th or spontaneous fission of ^{238}U. Thermal
296 neutrons are generated during (α, n) reactions, and by cosmic ray spallation, termed cosmic ray
297 thermal (CTN) neutrons (Dunai et al. 2007). The effect of these reactions is shown in Fig. 1.

298 The concentration of target elements F and Mg are negligible in quartz, so the dominant
299 nucleogenic Ne production is ^{18}O(α,n)^{21}Ne. Addition of this mono-isotopic component tends to
300 produce data that plot to the right of the air-spallation line in the neon three-isotope diagram (Fig. 1).
301 U and Th concentrations are typically low in pure quartz, but are often located in accessory mineral
302 inclusions, e.g., biotite, apatite and zircon (Schäfer et al. 2002). α-particles recoil 10-40 μm during
303 production, and can be implanted into the outer few 10's μm of grains. As the nucleogenic Ne is
304 located in the crystal lattice of quartz, it is released with cosmogenic neon predominantly below
305 800°C. The removal of the rims of quartz grains by acid etching can reduce the nucleogenic
306 component (Kohl and Nishiizumi 1992). On the other analysis of shielded samples with the exposed
307 lithology can be used to quantify the contribution of non-cosmogenic nuclides (e.g., Margerison et al.
308 2005).

309 Crustal fluids are typically enriched in nucleogenic ^{21}Ne and ^{22}Ne, acquired by water-rock

interaction during fluid circulation in the crust (Kennedy et al. 1990). When these fluids are trapped as inclusions in minerals they impart nucleogenic Ne. The isotopic composition of the fluid depends on O/F ratio of the crust (Ballentine and Burnard 2002; Kennedy et al. 1990). Kennedy et al. (1990) has shown that crustal fluids typically have higher $^{22}Ne/^{21}Ne$ ratios than that of cosmogenic Ne (Fig. 1) but it may not always be possible to distinguish cosmogenic neon. Usually the inclusion-hosted volatiles require higher release temperatures than cosmogenic Ne during stepwise heating experiments and it may be possible to separate the two components and allow cosmogenic Ne to be quantified (Niedermann et al. 1994).

Mantle Ne: Mantle-derived neon is enriched in ^{20}Ne and ^{21}Ne relative to air Ne. It is typically incorporated in magmatic minerals at the time of rock formation, and usually dominantly present as melt or vapour inclusions. It should be clearly identified because of its distinct isotopic composition, whose trend is almost perpendicular to the spallation line (Fig. 1).

Inherited cosmogenic Ne: Cosmogenic Ne that has been produced prior to the exposure event that brought rocks to the surface will not, in contrast to the radionuclides, decay away. It will be isotopically indistinguishable from the modern cosmogenic Ne and, if not identified, will exaggerate exposure durations and lower erosion rates. While it is widely recognized in attempts to date the deposition of modern sediments (e.g., Ma et al. 2016), it is also likely to be a problem in the analysis of bedrock and boulders made of sedimentary or meta-sedimentary rocks which may be composed of detrital quartz that was exposed during erosion and transport of the grains that made up the sediment prior to lithification.

There are several approaches to determining the amount of cosmogenic Ne in a mineral. The commonest is to quantify and remove the atmospheric ^{21}Ne:

$$^{21}Ne_{ex} = {}^{20}Ne_{mea} \times \left[\left({}^{21}Ne / {}^{20}Ne \right)_{mea} - \left({}^{21}Ne / {}^{20}Ne \right)_{air} \right] \qquad (6)$$

where $^{21}Ne_{ex}$ is typically a mixture of *in situ* and crustal nucleogenic Ne, and cosmogenic Ne. The non-cosmogenic (mantle and nucleogenic) component of the excess ^{21}Ne can be measured in deeply shielded samples of the same lithology as analysed for cosmogenic Ne. In modern sedimentary deposits the cosmogenic Ne generated during erosion and transport can be determined using the depth

profile method (Anderson et al. 1996; Hetzel et al. 2002a). If no post-depositional displacement of the deposit has occurred, and the transport and depositional processes were invariant in the sedimentary sequence, the concentration of cosmogenic Ne should decrease exponentially with depth, and a concentration versus depth plot should asymptotically approach the mean inheritance at depths of greater than 2 meters (Fig. 3) (e.g., Ma et al. 2016). Other approaches to correcting for nucleogenic Ne concentrations include calculating the *in situ* contribution from measured radioelement concentrations and the algorithm of Yatsevich and Honda (1997), and using the measured radiogenic ^{40}Ar and/or fissiogenic Xe isotopes to quantify the amount of trapped crustal ^{21}Ne (e.g., Fujioka et al. 2005).

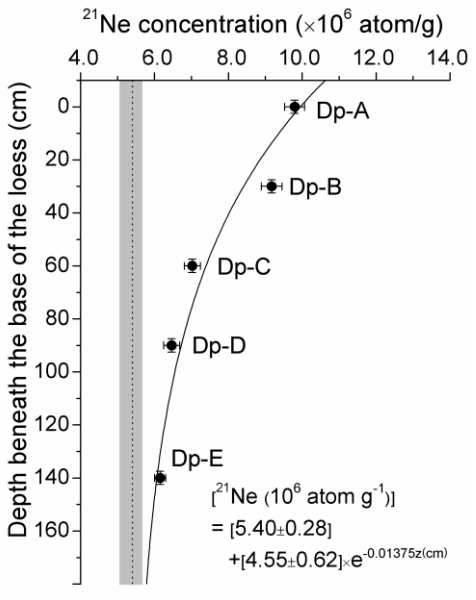

Fig. 3 The cosmogenic ^{21}Ne concentration profile, showing the amount of ^{21}Ne inheritance in terrace deposits (Ma et al. 2016). Error bars represent 1σ uncertainties. The black curve is the fitted exponential function. The dashed line and the margins of the light gray band correspond to the value of ^{21}Ne inheritance and its error boundaries

5. Applications of cosmogenic Ne

5.1 Exposure age determinations under independent constraint on erosion rate

The presence of non-cosmogenic neon components in minerals adds uncertainty to the accuracy of exposure age determined by cosmogenic ^{21}Ne. Nevertheless, cosmogenic ^{21}Ne is produced and

356 retained in a range of minerals and thus has the potential for constraining the timing of the exposure
357 of surfaces that cannot be studied with ^{10}Be, ^{26}Al and ^{36}Cl.

358 Cosmogenic ^{3}He, in olivine and pyroxene phenocrysts, has been widely applied for dating the
359 eruption of Pleistocene and Holocene basalt lavas where ^{14}C-datable material is not present (e.g.,
360 Foeken et al. 2009; Kurz 1986). Helium isotope determinations are easier than neon isotopes, and
361 uncertainties associated with ^{3}He-derived exposure ages are typically lower than those from
362 cosmogenic ^{21}Ne. In several studies cosmogenic ^{21}Ne has also been measured on the same samples in
363 order to confirm the ^{3}He-derived exposure ages (Espanon et al. 2014; Fenton and Niedermann 2014;
364 Gillen et al. 2010; Sarda et al. 1993; Staudacher and Allègre 1993). However, helium has only two
365 isotopes, and thus the correction for non-cosmogenic components is complex. The three Ne isotopes
366 allows a more effective resolution of the contribution from cosmogenic component (e.g., Staudacher
367 and Allègre 1993), but it is still difficult to detect small amounts of cosmogenic ^{21}Ne in the presence
368 of relatively large amount of non-cosmogenic ^{21}Ne.

369 As well as dating the eruption age of basalts, the cosmogenic noble gas isotopes can be used for
370 determining the time that basalts were eroded. Cerling et al. (1994) determined the timing of flood
371 events by measuring the cosmogenic ^{3}He and ^{21}Ne exposure ages of eroded basalt boulders and
372 scoured bedrock of the Big Lost River on the Snake Piver Plain, Colorado. However, they noted that
373 flood surface samples had a range of cosmogenic ^{3}He and ^{21}Ne concentrations. A small number of the
374 surface samples appear to have slightly higher concentrations, consistent with the inheritance of
375 cosmogenic nuclides that were produced prior the exposure of new surface during the flooding.

376 Cosmogenic radionuclides are commonly used for study of glacial histories (e.g., Ivy-Ochs et al.
377 1995). Cosmogenic ^{21}Ne has been less commonly exploited in the study of glacial landforms yet holds
378 huge potential. Graf et al. (2007) used cosmogenic ^{10}Be and ^{21}Ne to date erratic boulders from the top
379 of the Montoz anticline in the Jura Mountains, Switzerland, to establish the pre-LGM glacial history.
380 Strasky et al. (2009b) used ^{10}Be and ^{21}Ne to show the continuous long-term exposure history of the
381 erratic boulders in southern Tibet, and investigated how sensitive the glacial system is to the North
382 Atlantic climate forcing.

383 Cosmogenic ^{21}Ne has also been used to determine the time of sediment deposition, such as river

terraces and alluvial fans. It is used in particular to confirm the simple exposure history of the sediment surface, ruling out periods of burial, and to correct for the cosmogenic ^{10}Be that is generated during erosion of bedrock and transport of the clasts to the site of sedimentation. Phillips et al. (1998) reported cosmogenic ^{21}Ne analysis of quartz sand derived from the Quaternary Bandelier Tuff to estimate the depositional ages of alluvium and soils on the alluvial plateau in New Mexico. They employed a depth profile to constrain the concentration of inherited ^{21}Ne and determine the inheritance- and burial-corrected ^{21}Ne exposure ages for individual surfaces of two terraces. Hetzel et al. (2002a) used ^{21}Ne to determine the exposure age of fluvial terraces, and demonstrated the importance of determining the trapped (non-cosmogenic) Ne components in samples. Cosmogenic Ne measured in boulders on ancient marine terraces from northern Spain has been used to determine the tectonic history (Alvarez-Marrón et al. 2008). The long exposure history, 1-2 million years, includes periods of burial and suggested that the wave-cut platform was generated in the Pliocene, and then the uplift in response to crustal deformation.

Codilean et al. (2008) tested the hypothesis that there is spatial variation in erosion in a river catchment by measuring cosmogenic Ne in 32 quartz pebbles in the Gaub River catchment, Namibia. This data was compared to distribution predicted using measured catchment-averaged erosion rates and the mean slope values. The ^{21}Ne concentrations span nearly two orders of magnitude and are skewed to low values consistent with predicted patterns, which imply that the measured distribution is a signature of the spatial variation in erosion rates.

Later, Kober et al. (2009) employed ^{10}Be, ^{26}Al, and ^{21}Ne in river sand quartz from Rio Lluta catchment in the arid area of northern Chile to determine catchment-wide denudation rates. Denudation rates derived from ^{21}Ne gave lowest rates (12-17 m Ma^{-1}). By comparing the catchment-wide ^{21}Ne-derived erosion rate with the headwater region erosion rates derived from ^{21}Ne/^{10}Be and ^{26}Al/^{10}Be nuclide pairs, the authors highlighted ^{21}Ne can be used to determine the temporal variation in sediment transport processes.

Antón et al. (2012) used cosmogenic ^{10}Be and ^{21}Ne to understand the Cenozoic history of the Duero River in the Arribes Gorge. Exposure ages for surfaces at various levels in the incised Duero River suggests that the final 2–300 m of fluvial incision in the Arribes Gorge occurred at a rate of 2–3

412 mm/yr over the last ~100 ka.

413 The different half-lives of ^{10}Be and ^{26}Al have been exploited to determine the duration of sediment
414 burial, which can be used to determine sedimentation age and deposition rates (e.g., Balco and Stone
415 2005; Granger et al. 1997). Balco and Shuster (2009a) first reported the incorporation of ^{21}Ne into the
416 burial dating method to date cave sediments from the Riverbluff Cave in Springfield and the
417 sedimentation age of Whippoorwill formation at the Pendleton clay pit near Pendleton, Missouri,
418 USA. The authors established the feasibility of this method and showed the improved age range and
419 accuracy of ^{10}Be/^{21}Ne nuclide pair comparing to that of ^{10}Be/^{26}Al. Subsequently Davis et al. (2011)
420 applied ^{10}Be, ^{26}Al and ^{21}Ne to date the burial age of the late Neogene sedimentary formations from
421 central Jordan Valley, Israel. They obtained an age range from 3.5 to 5.3 Ma for Pliocene-early
422 Pleistocene lacustrine sediments. This provided them with independent age constraints that were used
423 in combination with magnetostratigraphy to understand the depositional history. Matmon et al. (2014)
424 employed ^{21}Ne, ^{10}Be and ^{26}Al to date the sedimentary sequences deposited in the Sedom Lagoon to
425 investigate the rift-forming and escarpment evolution along the Dead Sea fault, which reflects the
426 Neogene development of the relative African-Arabian plate motion.

427 Low-relief bedrock surfaces typically occur at high altitude, and are commonly interpreted as
428 remnants of palaeo-surfaces that had originally a much larger extent (e.g., Clark et al. 2005). The
429 bedrock peneplains can be used to infer significant amount of rock uplift after their generation at low
430 elevation. However, the duration of such surfaces was preserved at high elevation and the rate at
431 which they were modified by erosion are difficult to be quantified. Strobl et al. (2012) combined ^{21}Ne
432 and ^{10}Be data measured in quartz clasts to confirm the simple exposure history with low denudation
433 rates (5-11 m Ma^{-1}) of the peneplain in north of Nam Co of the southern Tibetan Plateau, which
434 indicates the stability of exposure history and landscape evolution in this area.

435 The potential of cosmogenic nuclide dating method not only provides the chronology of geological
436 events, but in addition to offer the information about the rates of erosion and landscape evolution.
437 Hetzel et al. (2002b) determined the long-term slip rate of the active faults in Central Asia (~0.35 mm
438 a^{-1}) based on the ^{21}Ne, ^{10}Be and ^{26}Al exposure ages of the offset landforms. They noted that the rate is
439 two orders of magnitude slower than earlier estimates based on the assumption ages of the Last

Glacial Maximum, which indicated the long-term preservation of the geomorphic features in Central Asia. Goethals et al. (2009b) investigated the impact of faulting on erosion rates in low-relief landscape in the Bishop Tuff, California, using *in situ* ^{21}Ne in quartz from an ignimbrite with a known eruption age of 760 ± 2 ka. Under the steady-state erosion assumption, they obtained a series of erosion rates of the sites with various fault activities, which suggested that tectonic activity does not affect erosion rates in a recognizable way in the low-relief landscape. Ma et al. (2016) employed ^{21}Ne to measure the long-term average surface erosion rate at the Shapotou area in the northern margin of the Tibetan Plateau. They confirmed the steady-state erosion for cosmogenic ^{21}Ne in the sediment of this area by measuring the ^{21}Ne concentrations in quartz collected from a series of river terraces. The same ^{21}Ne concentrations within measurement uncertainties in the highest two terraces only provided the information about the erosion rate (0.54-0.72 cm ka^{-1}) instead of the exposure duration of terraces.

Perhaps the most exciting potential for cosmogenic ^{21}Ne exposure dating is its application for understanding the surface history of other planets. The lack of need for performing chemistry can allow nuclide determinations in planet surfaces, ruling out the need for sample return missions. In the first study of this kind, Farley et al. (2014) used the Sample Analysis at Mars (SAM) instrument on the Curiosity rover to determine the concentration of cosmogenic ^{3}He, ^{21}Ne and ^{36}Ar in a mudstone from the floor of Gale Crater on Mars. They obtained consistent exposure ages from different isotopes with an average value of 78 ± 30 million years. Comparing with the formation age (4.21 ± 0.35 billion years) of the rocks comprising the crater rim, which is constrained by K-Ar dating, the authors drew the scarp retreat hypothesis which caused the recent exposure of the mudstone after long-term burial from its deposition. The large uncertainty reflects the difficulty of making these measurements, and assumptions regarding the cosmic ray flux, but it shows a novel perspective for applications of cosmogenic noble gas isotopes in many new fields of Earth sciences and beyond in near future.

5.2 Long-term landscape development in low erosion rate regions

The presence of air-derived Ne and nucleogenic ^{21,22}Ne in quartz, means that cosmogenic Ne requires approximately 10 times longer exposure than required for ^{10}Be to obtain the equivalent precision and accuracy. Consequently most landscape elements from temperate climates that are

468 theoretically datable with cosmogenic ^{21}Ne are prone to surface erosion. As a result, cosmogenic ^{21}Ne
469 concentrations in landscape elements that are older than a few tens of thousands of years rarely reflect
470 the timing of formation. Landscape elements from low erosion rate regions, e.g. where climate is arid
471 and/or dry, can be preserved for millions of years, though on these timescales processes of burial and
472 exhumation may complicate the exposure histories. Cosmogenic ^{21}Ne is ideally suited for
473 understanding the evolution history and stability of erosional and depositional landforms. Here we
474 highlight two extensively studied regions: Antarctica and the High Andes of Peru and Chile.

475 Cosmogenic ^{21}Ne has proved powerful tool for reconstructing the Plio-Pleistocene history of
476 Antarctica glaciations, specifically understanding the glacial volume fluctuations on both temporal
477 and spatial scales, and addressing whether the Antarctic climate is decoupled from global climate
478 variations or has been subject to similar fluctuations as took place elsewhere on the planet, i.e. the
479 dynamic and stable glaciations variation hypothesis about the climatic change in Antarctica. The
480 extremely low erosion rates in the Dry Valleys allows the cosmogenic nuclide exposure dating to be
481 accurately applied over a much longer time range, which is up to millions of years. Several studies
482 have focused on dating the glacial advances and establishing the association of the ancient glacial
483 landforms with the Antarctic climate changes (e.g., Bruno et al. 1997; Kong et al. 2010; Schäfer et al.
484 1999; Van der Wateren et al. 1999). Many of these studies have exploited pyroxene from Ferrar
485 dolerite bedrock and boulders rather than quartz.

486 Exposure ages of ~6.5 Ma for doleritic clasts from Sirius tillite at Mount Fleming constrained the
487 uplift rates of the Transantarctic Mountain less than 170 m Ma^{-1} (Bruno et al. 1997). Extraordinarily
488 high surface exposure ages of 10 Ma for dolerite boulder from Mount Fleming obtained by Schäfer et
489 al. (1999) and 11.2 Ma for the bedrock sample from Daniels Range obtained by Van der Wateren et al.
490 (1999) support the hypothesis of a stable East Antarctic Ice Sheet since at least Late Miocene time and
491 imply the decoupled climate variations of Antarctica from lower southern latitude regions.

492 Summerfield et al. (1999) first focused on measuring surface process rates of this extremely old
493 landscape, and they estimated the long-term denudation rate in the Dry Valleys area of the
494 Transantarctic Mountains, southern Victoria Land from the concentrations of cosmogenic ^{21}Ne
495 measured in quartz in both sandstones and granitic basement. The denudation rates were proved

sensitive to the landform elements, ranging from 0.26-1.02 m Ma^{-1} for the rectilinear slopes down to 0.133-0.164 m Ma^{-1} for the high-elevation surface sites. Oberholzer et al. (2003) combined ^{21}Ne with ^{3}He, and ^{10}Be to limit Plio-Pleistocene glaciations in the Deep Freeze Range in northern Victoria Land. They measured surface exposure ages and erosion rates of both the bedrock and glacial erratic, and taking into account the erosion rate of 20 cm Ma^{-1}, they obtained a mid-Pliocene exposure age of the landscape surface in the McMurdo Dry Valleys, which indicates a constantly cold and hyperarid climate in this area. Surface cobbles on moraines in the Vemier Valley, located at the inland edge of the Dry Valleys region were analyzed to provide age control of the glacier activity by Staiger et al. (2006). They used a conservative erosion rate of 5 cm Ma^{-1} in age calculations, and obtained a series of cosmogenic ^{21}Ne exposure ages of old moraines of Ferrar dolerite. Subsequently, they used one of modern moraines cobbles sample to constrain the inheritance component in old moraines, and the cosmogenic age for the modern moraine suggested a value for nuclide inheritance of about 50 kyr, which was less than 5% of the total exposure time of the oldest boulders.

To address the response of Antarctic ice sheets to global climate changes, Oberholzer et al. (2008) measured ^{21}Ne concentrations in the rock surfaces on nunataks in northern Victoria Land to investigate the duration of exposure generated by the glacial activity on the surfaces of nunataks. They gave the first absolute ages of 3.5 Ma of this area, which recorded the ice-free duration in this area. Strasky et al. (2009a) determined the exposure ages of the erratic boulders taking the surface erosion into account, and the dating results implied the low-amplitude Pleistocene variations in East Antarctic Ice Sheet, Victoria Land. Kong et al. (2010) applied the multiple nuclides ^{21}Ne-^{10}Be-^{26}Al to fit the surface exposure age of the bedrock on the Mount Harding to ~6.3 Ma, which recorded the time of the East Antarctic Ice Sheet retreated below the summit of the Mount Harding and suggested the important impact of the moisture transport from the Southern Ocean on the ice sheet expansion in the interior of East Antarctica. Altmaier et al. (2010) reported a series of rock exposure ages for the Queen Maud Land, Antarctica. They used ^{21}Ne to date the samples in which radionuclide concentrations had nearly been saturated, and obtained minimum ^{21}Ne exposure ages longer than 8 Ma, which excludes the presence of warm and humid climatic conditions during this period. Recently, Hein et al. (2016) present geomorphological evidence and multiple cosmogenic nuclide data from the

southern Ellsworth Mountains to suggest that the divide of the West Antarctic Ice Sheet has fluctuated only modestly in location and thickness for at least the last 1.4 million years.

The western central Andes are tectonically active and in situ cosmogenic nuclides allow the relationship between erosion, tectonics and climate on landscape evolution to be determined. The Atacama Desert is the driest place on Earth, and the onset of the aridification of the Atacama has been reported to be from at least the late Miocene (Dunai et al. 2005), which is indicated by the ^{21}Ne ages ranging from 9 Ma to 37 Ma of individual clasts on depositional surfaces. To investigate whether the slow landscape evolution is characteristic of the entire Atacama, or only of specific regions, or landscape elements, Placzek et al. (2010) employed ^{10}Be, ^{26}Al and ^{21}Ne to quantify the exposure history of a wide variety of landscape elements, including bedrock, alluvial fans, stream sediment and boulders, along a transect across the Central Atacama. Their dating results as well as the field observations indicate the Central Atacama is more active than the Northern Atacama, and has remained geomorphically active well into the Pleistocene.

6. Perspective

In the past few decades *in situ* produced cosmogenic ^{21}Ne has found a broad range of applications in many fields of Earth surface processes studies. Most of these studies have utilised quartz. However the retention of cosmogenic ^{21}Ne in most other silicate and oxide minerals will no doubt open new areas of surface process research.

Developments in the ability to precisely measure smaller amounts of Ne will continue. Newly developed amplifiers with 10^{12} and 10^{13} Ω feedback resistors with fast response times and low noise characteristics offer the possibility of more stable measurement of small ion beam currents, and improved measurement precision. Combined Faraday-electron multiplier detectors will provide flexibility in analysis protocols. Increased resolution of new generation noble gas mass spectrometers is starting to provide separation of isobaric interferences and thus more accurate and precise measurement. This has, so far, extended as far as separation of $^{20}Ne^{+}$ and $^{40}Ar^{2+}$. Laser heating systems minimize the noble gases blanks and hence will lower detection limits, and allow precise and accurate measurements from smaller samples.

552

553 **Conflict of Interest:**

554 The authors declare that they have no conflict of interest.

555

556 **References**

557 Altmaier M, Herpers U, Delisle G, Merchel S, Ott U (2010) Glaciation history of Queen Maud Land
558 (Antarctica) reconstructed from in-situ produced cosmogenic ^{10}Be, ^{26}Al and ^{21}Ne. Polar Science
559 4:42-61

560 Alvarez-Marrón J, Hetzel R, Niedermann S, Menéndez R, Marquínez J (2008) Origin, structure and
561 exposure history of a wave-cut platform more than 1 Ma in age at the coast of northern Spain: a
562 multiple cosmogenic nuclide approach. Geomorphology 93:316-334

563 Anderson RS, Repka JL, Dick GS (1996) Explicit treatment of inheritance in dating depositional
564 surfaces using in situ ^{10}Be and ^{26}Al. Geology 24:47-51

565 Antón L et al. (2012) Quantification of fluvial incision in the Duero Basin (NW Iberia) from
566 longitudinal profile analysis and terrestrial cosmogenic nuclide concentrations. Geomorphology
567 165:50-61

568 Balco G, Shuster DL (2009a) ^{26}Al–^{10}Be–^{21}Ne burial dating. Earth Planet Sci Lett 286:570-575

569 Balco G, Shuster DL (2009b) Production rate of cosmogenic ^{21}Ne in quartz estimated from ^{10}Be, ^{26}Al,
570 and ^{21}Ne concentrations in slowly eroding Antarctic bedrock surfaces. Earth Planet Sci Lett
571 281:48-58

572 Balco G, Stone JO (2005) Measuring middle Pleistocene erosion rates with cosmic-ray-produced
573 nuclides in buried alluvial sediment, Fisher Valley, southeastern Utah. Earth Surf Process Landf
574 30:1051-1067

575 Balco G, Stone JO, Lifton NA, Dunai TJ (2008) A complete and easily accessible means of
576 calculating surface exposure ages or erosion rates from ^{10}Be and ^{26}Al measurements. Quat
577 Geochronol 3:174-195

578 Ballentine CJ, Burnard PG (2002) Production, release and transport of noble gases in the continental
579 crust. Rev Mineral Geochem 47:481-538

580 Barbouti A, Rastin B (1983) A study of the absolute intensity of muons at sea level and under various
581 thicknesses of absorber. J Phys G: Nucl Phys 9:1577-1595
582 Benedetti L et al. (2002) Post-glacial slip history of the Sparta fault (Greece) determined by ^{36}Cl
583 cosmogenic dating: Evidence for non-periodic earthquakes. Geophys Res Lett 29.
584 doi:10.1029/2001GL014510
585 Borchers B et al. (2016) Geological calibration of spallation production rates in the CRONUS-Earth
586 project. Quat Geochronol 31:188-198
587 Braucher R, Merchel S, Borgomano J, Bourlès D (2011) Production of cosmogenic radionuclides at
588 great depth: a multi element approach. Earth Planet Sci Lett 309:1-9
589 Brown ET, Bourlès D, Colin F, Raisbeck GM, Yiou F, Desgarceaux S (1995) Evidence for muon-
590 induced production of ^{10}Be in near-surface rocks from the Congo. Geophys Res Lett 22:703-706
591 Bruno LA, Baur H, Graf T, Schlu C, Signer P, Wieler R (1997) Dating of Sirius group tillites in the
592 Antarctic Dry Valleys with cosmogenic ^{3}He and ^{21}Ne. Earth Planet Sci Lett 147:37-54
593 Cerling TE, Poreda RJ, Rathburn SL (1994) Cosmogenic ^{3}He and ^{21}Ne age of the big lost river flood,
594 Snake River plain, Idaho. Geology 22:227-230
595 Clark DH, Bierman PR, Larsen P (1995) Improving in situ cosmogenic chronometers. Quat Res
596 44:367-377
597 Clark MK, House M, Royden L, Whipple K, Burchfiel B, Zhang X, Tang W (2005) Late Cenozoic
598 uplift of southeastern Tibet. Geology 33:525-528
599 Codilean AT, Bishop P, Stuart FM, Hoey TB, Fabel D, Freeman SP (2008) Single-grain cosmogenic
600 ^{21}Ne concentrations in fluvial sediments reveal spatially variable erosion rates. Geology 36:159-
601 162
602 Davis M, Matmon A, Fink D, Ron H, Niedermann S (2011) Dating Pliocene lacustrine sediments in
603 the central Jordan Valley, Israel—Implications for cosmogenic burial dating. Earth Planet Sci
604 Lett 305:317-327
605 Desilets D, Zreda M (2003) Spatial and temporal distribution of secondary cosmic-ray nucleon
606 intensities and applications to in situ cosmogenic dating. Earth Planet Sci Lett 206:21-42
607 Desilets D, Zreda M, Prabu T (2006) Extended scaling factors for in situ cosmogenic nuclides: new

measurements at low latitude. Earth Planet Sci Lett 246:265-276

Dunai T (2001) Influence of secular variation of the geomagnetic field on production rates of in situ produced cosmogenic nuclides. Earth Planet Sci Lett 193:197-212

Dunai TJ, López GAG, Juez-Larré J (2005) Oligocene–Miocene age of aridity in the Atacama Desert revealed by exposure dating of erosion-sensitive landforms. Geology 33:321-324

Dunai TJ, Stuart FM, Pik R, Burnard P, Gayer E (2007) Production of ^{3}He in crustal rocks by cosmogenic thermal neutrons. Earth Planet Sci Lett 258:228-236

Eberhardt P, Eugster O, Marti K (1965) Notizen: A Redetermination of the Isotopic Composition of Atmospheric Neon. Z Naturforsch A 20:623-624

Espanon VR, Honda M, Chivas AR (2014) Cosmogenic ^{3}He and ^{21}Ne surface exposure dating of young basalts from Southern Mendoza, Argentina. Quat Geochronol 19:76-86

Evenstar LA, Stuart FM, Hartley AJ, Tattitch B (2015) Slow Cenozoic uplift of the western Andean Cordillera indicated by cosmogenic ^{3}He in alluvial boulders from the Pacific Planation Surface. Geophys Res Lett 42:8448-8455

Farley K et al. (2014) In situ radiometric and exposure age dating of the Martian surface. science 343:1247166

Fenton CR, Niedermann S (2014) Surface exposure dating of young basalts (1–200 ka) in the San Francisco volcanic field (Arizona, USA) using cosmogenic ^{3}He and ^{21}Ne. Quat Geochronol 19:87-105

Foeken JP, Day S, Stuart FM (2009) Cosmogenic ^{3}He exposure dating of the Quaternary basalts from Fogo, Cape Verdes: implications for rift zone and magmatic reorganisation. Quat Geochronol 4:37-49

Foeken JP, Stuart FM, Mark DF (2012) Long-term low latitude cosmogenic ^{3}He production rate determined from a 126 ka basalt from Fogo, Cape Verdes. Earth Planet Sci Lett 359:14-25

Fujioka T, Chappell J, Honda M, Yatsevich I, Fifield K, Fabel D (2005) Global cooling initiated stony deserts in central Australia 2–4 Ma, dated by cosmogenic ^{21}Ne-^{10}Be. Geology 33:993-996

Gillen D, Honda M, Chivas AR, Yatsevich I, Patterson D, Carr PF (2010) Cosmogenic ^{21}Ne exposure dating of young basaltic lava flows from the Newer Volcanic Province, western Victoria,

636 Australia. Quat Geochronol 5:1-9
637 Goehring BM, Kurz MD, Balco G, Schaefer JM, Licciardi J, Lifton N (2010) A reevaluation of in situ
638 cosmogenic ^{3}He production rates. Quat Geochronol 5:410-418
639 Goethals M et al. (2009a) An improved experimental determination of cosmogenic ^{10}Be/^{21}Ne and
640 ^{26}Al/^{21}Ne production ratios in quartz. Earth Planet Sci Lett 284:187-198
641 Goethals M, Niedermann S, Hetzel R, Fenton C (2009b) Determining the impact of faulting on the
642 rate of erosion in a low-relief landscape: A case study using in situ produced ^{21}Ne on active
643 normal faults in the Bishop Tuff, California. Geomorphology 103:401-413
644 Gosse JC, Phillips FM (2001) Terrestrial in situ cosmogenic nuclides: theory and application. Quat
645 Sci Rev 20:1475-1560
646 Graf AA, Strasky S, Ivy-Ochs S, Akçar N, Kubik PW, Burkhard M, Schlüchter C (2007) First results
647 of cosmogenic dated pre-Last Glaciation erratics from the Montoz area, Jura Mountains,
648 Switzerland. Quat Int 164:43-52
649 Graf T, Kohl C, Marti K, Nishiizumi K (1991) Cosmic-ray produced neon in Antarctic rocks.
650 Geophys Res Lett 18:203-206
651 Granger D, Riebe C (2007) Cosmogenic nuclides in weathering and erosion. Treatise on geochemistry
652 5:1-43
653 Granger DE, Kirchner JW, Finkel RC (1997) Quaternary downcutting rate of the New River, Virginia,
654 measured from differential decay of cosmogenic ^{26}Al and ^{10}Be in cave-deposited alluvium.
655 Geology 25:107-110
656 Granger DE, Smith AL (2000) Dating buried sediments using radioactive decay and muogenic
657 production of ^{26}Al and ^{10}Be. Nucl Instrum Methods Phys Res B 172:822-826
658 Hein AS et al. (2016) Evidence for the stability of the West Antarctic Ice Sheet divide for 1.4 million
659 years. Nat Commun 7:10325
660 Hetzel R, Niedermann S, Ivy-Ochs S, Kubik PW, Tao M, Gao B (2002a) ^{21}Ne versus ^{10}Be and ^{26}Al
661 exposure ages of fluvial terraces: the influence of crustal Ne in quartz. Earth Planet Sci Lett
662 201:575-591
663 Hetzel R, Niedermann S, Tao M, Kubik PW, Ivy-Ochs S, Gao B, Strecker MR (2002b) Low slip rates

664 and long-term preservation of geomorphic features in Central Asia. Nature 417:428-432
665 Honda M, Zhang X, Phillips D, Hamilton D, Deerberg M, Schwieters JB (2015) Redetermination of
666 the ^{21}Ne relative abundance of the atmosphere, using a high resolution, multi-collector noble gas
667 mass spectrometer (HELIX-MC Plus). Int J Mass Spectrom 387:1-7
668 Ivy-Ochs S et al. (2006) The timing of glacier advances in the northern European Alps based on
669 surface exposure dating with cosmogenic ^{10}Be, ^{26}Al, ^{36}Cl, and ^{21}Ne. Geol Soc Am Spec Pap
670 415:43-60
671 Ivy-Ochs S, Schlüchter C, Kubik PW, Dittrich-Hannen B, Beer J (1995) Minimum ^{10}Be exposure ages
672 of early Pliocene for the Table Mountain plateau and the Sirius Group at Mount Fleming, Dry
673 Valleys, Antarctica. Geology 23:1007-1010
674 Kennedy B, Hiyagon H, Reynolds J (1990) Crustal neon: a striking uniformity. Earth Planet Sci Lett
675 98:277-286
676 Kober F, Ivy-Ochs S, Zeilinger G, Schlunegger F, Kubik P, Baur H, Wieler R (2009) Complex
677 multiple cosmogenic nuclide concentration and histories in the arid Rio Lluta catchment,
678 northern Chile. Earth Surf Process Landf 34:398-412
679 Kohl C, Nishiizumi K (1992) Chemical isolation of quartz for measurement of in-situ-produced
680 cosmogenic nuclides. Geochimica et Cosmochimica Acta 56:3583-3587
681 Kong P, Huang F, Liu X, Fink D, Ding L, Lai Q (2010) Late Miocene ice sheet elevation in the Grove
682 Mountains, East Antarctica, inferred from cosmogenic ^{21}Ne–^{10}Be–^{26}Al. Glob Planet Change
683 72:50-54
684 Kurz MD (1986) In situ production of terrestrial cosmogenic helium and some applications to
685 geochronology. Geochimica et Cosmochimica Acta 50:2855-2862
686 Lal D (1991) Cosmic ray labeling of erosion surfaces: in situ nuclide production rates and erosion
687 models. Earth Planet Sci Lett 104:424-439
688 Lal D, Peters B (1967) Cosmic ray produced radioactivity on the earth. In: Sitte K (ed) Cosmic Rays.
689 Springer, Berlin Heidelberg, pp 551-612
690 Lifton N, Sato T, Dunai TJ (2014) Scaling in situ cosmogenic nuclide production rates using
691 analytical approximations to atmospheric cosmic-ray fluxes. Earth Planet Sci Lett 386:149-160

Lifton NA, Bieber JW, Clem JM, Duldig ML, Evenson P, Humble JE, Pyle R (2005) Addressing solar modulation and long-term uncertainties in scaling secondary cosmic rays for in situ cosmogenic nuclide applications. Earth Planet Sci Lett 239:140-161

Ma Y, Wu Y, Li D, Zheng D (2015) Analytical procedure of neon measurements on GV 5400 noble gas mass spectrometer and its evaluation by quartz standard CREU-1. Int J Mass Spectrom 380:26-33

Ma Y et al. (2016) Erosion rate in the Shapotou area, northwestern China, constrained by in situ-produced cosmogenic ^{21}Ne in long-exposed erosional surfaces. Quat Geochronol 31:3-11

Margerison H, Phillips W, Stuart F, Sugden D (2005) An assessment of cosmogenic ^{3}He surface exposure dating in the Northern Dry Valleys of East Antarctica. Earth Planet Sci Lett 230:163-175

Marrero SM, Phillips FM, Borchers B, Lifton N, Aumer R, Balco G (2016) Cosmogenic nuclide systematics and the CRONUScalc program. Quat Geochronol 31:160-187

Masarik J, Reedy RC (1995) Terrestrial cosmogenic-nuclide production systematics calculated from numerical simulations. Earth Planet Sci Lett 136:381-395

Matmon A, Fink D, Davis M, Niedermann S, Rood D, Frumkin A (2014) Unraveling rift margin evolution and escarpment development ages along the Dead Sea fault using cosmogenic burial ages. Quat Res 82:281-295

Niedermann S (2000) The ^{21}Ne production rate in quartz revisited. Earth Planet Sci Lett 183:361-364

Niedermann S (2002) Cosmic-ray-produced noble gases in terrestrial rocks: dating tools for surface processes. Rev Mineral Geochem 47:731-784

Niedermann S, Graf T, Kim J, Kohl C, Marti K, Nishiizumi K (1994) Cosmic-ray-produced ^{21}Ne in terrestrial quartz: the neon inventory of Sierra Nevada quartz separates. Earth Planet Sci Lett 125:341-355

Niedermann S, Graf T, Marti K (1993) Mass spectrometric identification of cosmic-ray-produced neon in terrestrial rocks with multiple neon components. Earth Planet Sci Lett 118:65-73

Nishiizumi K, Winterer E, Kohl C, Klein J, Middleton R, Lal D, Arnold J (1989) Cosmic ray production rates of ^{10}Be and ^{26}Al in quartz from glacially polished rocks. J Geophys Res Solid

720 Earth 94:17907-17915
721 Oberholzer P, Baroni C, Salvatore M, Baur H, Wieler R (2008) Dating late Cenozoic erosional
722 surfaces in Victoria Land, Antarctica, with cosmogenic neon in pyroxenes. Antarct Sci 20:89-98
723 Oberholzer P et al. (2003) Limited Pliocene/Pleistocene glaciation in Deep Freeze Range, northern
724 Victoria Land, Antarctica, derived from in situ cosmogenic nuclides. Antarct Sci 15:493-502
725 Phillips FM et al. (2016) The CRONUS-Earth project: a synthesis. Quat Geochronol 31:119-154
726 Phillips WM, McDonald EV, Reneau SL, Poths J (1998) Dating soils and alluvium with cosmogenic
727 ^{21}Ne depth profiles: case studies from the Pajarito Plateau, New Mexico, USA. Earth Planet Sci
728 Lett 160:209-223
729 Placzek C, Matmon A, Granger D, Quade J, Niedermann S (2010) Evidence for active landscape
730 evolution in the hyperarid Atacama from multiple terrestrial cosmogenic nuclides. Earth Planet
731 Sci Lett 295:12-20
732 Portenga EW, Bierman PR (2011) Understanding Earth's eroding surface with ^{10}Be. GSA Today 21:4-
733 10
734 Sarda P, Staudacher T, Allègre CJ, Lecomte A (1993) Cosmogenic neon and helium at Réunion:
735 measurement of erosion rate. Earth Planet Sci Lett 119:405-417
736 Schäfer JM, Ivy-Ochs S, Wieler R, Leya I, Baur H, Denton GH, Schlüchter C (1999) Cosmogenic
737 noble gas studies in the oldest landscape on earth: surface exposure ages of the Dry Valleys,
738 Antarctica. Earth Planet Sci Lett 167:215-226
739 Schäfer JM et al. (2002) The limited influence of glaciations in Tibet on global climate over the past
740 170 000 yr. Earth Planet Sci Lett 194:287-297
741 Shuster DL, Farley KA (2005) ^{4}He/^{3}He thermochronometry: theory, practice, and potential
742 complications. Rev Mineral Geochem 58:181-203
743 Staiger J, Marchant D, Schaefer J, Oberholzer P, Johnson J, Lewis A, Swanger K (2006) Plio-
744 Pleistocene history of Ferrar Glacier, Antarctica: Implications for climate and ice sheet stability.
745 Earth Planet Sci Lett 243:489-503
746 Staudacher T, Allègre CJ (1993) Ages of the second caldera of Piton de la Fournaise volcano
747 (Réunion) determined by cosmic ray produced ^{3}He and ^{21}Ne. Earth Planet Sci Lett 119:395-404

748 Stone J, Vasconcelos P (2000) Studies of geomorphic rates and processes with cosmogenic isotopes—
749 examples from Australia. J Conf Abs 5:961
750 Strasky S et al. (2009a) Surface exposure ages imply multiple low-amplitude Pleistocene variations in
751 East Antarctic ice sheet, Ricker Hills, Victoria Land. Antarct Sci 21:59-69
752 Strasky S, Graf AA, Zhao Z, Kubik PW, Baur H, Schlüchter C, Wieler R (2009b) Late Glacial ice
753 advances in southeast Tibet. J Asian Earth Sci 34:458-465
754 Strobl M, Hetzel R, Niedermann S, Ding L, Zhang L (2012) Landscape evolution of a bedrock
755 peneplain on the southern Tibetan Plateau revealed by in situ-produced cosmogenic ^{10}Be and
756 ^{21}Ne. Geomorphology 153:192-204
757 Summerfield M, Stuart F, Cockburn H, Sugden D, Denton G, Dunai T, Marchant D (1999) Long-term
758 rates of denudation in the Dry Valleys, Transantarctic Mountains, southern Victoria Land,
759 Antarctica based on in-situ-produced cosmogenic ^{21}Ne. Geomorphology 27:113-129
760 Van den Bogaard P, Schirnick C (1995) ^{40}Ar/^{39}Ar laser probe ages of Bishop Tuff quartz phenocrysts
761 substantiate long-lived silicic magma chamber at Long Valley, United States. Geology 23:759-
762 762
763 Van der Wateren FM, Dunai TJ, Van Balen RT, Klas W, Verbers AL, Passchier S, Herpers U (1999)
764 Contrasting Neogene denudation histories of different structural regions in the Transantarctic
765 Mountains rift flank constrained by cosmogenic isotope measurements. Glob Planet Change
766 23:145-172
767 Vermeesch P (2007) CosmoCalc: An Excel add-in for cosmogenic nuclide calculations. Geochem
768 Geophys Geosyst 8. doi:10.1029/2006GC001530
769 Vermeesch P et al. (2015) Interlaboratory comparison of cosmogenic ^{21}Ne in quartz. Quat Geochronol
770 26:20-28
771 Yatsevich I, Honda M (1997) Production of nucleogenic neon in the Earth from natural radioactive
772 decay. J Geophys Res Solid Earth 102:10291-10298
773